

1 **Solar FTIR measurements of NO<sub>x</sub> vertical distributions: - Part II):**  
2 **Experiment-based scaling factors describing the ~~diurnal~~-daytime**  
3 **increase-variation of stratospheric NO<sub>x</sub>**

4 Pinchas Nürnberg<sup>1</sup>, Sarah A. Strode<sup>2,3</sup>, and Ralf Sussmann<sup>1</sup>

5 <sup>1</sup>Karlsruhe Institute of Technology, IMK-IFU, Garmisch-Partenkirchen, Germany

6 <sup>2</sup>Goddard Earth Sciences Technology and Research (GESTAR-II), Morgan State University, Baltimore, MD, 21251 USA

7 <sup>3</sup>NASA Goddard Space Flight Center, Greenbelt, MD 20771, USA

8 *Correspondence to:* Pinchas Nürnberg ([pinchas.nuernberg@kit.edu](mailto:pinchas.nuernberg@kit.edu)) and Ralf Sussmann ([ralf.sussmann@kit.edu](mailto:ralf.sussmann@kit.edu))

9

10 **Abstract**

11 Long-term experimental stratospheric NO<sub>2</sub> and NO partial columns measured by means of solar Fourier-transform infrared  
12 (FTIR) spectrometry at Zugspitze (47.42° N, 10.98° E, 2964 m a.s.l.), Germany were used to create a set of experiment-based  
13 monthly scaling factors ( $SF_{exp}$ ). The underlying data set is published in a companion paper (Nürnberg et al., 2023) comprising  
14 over 25 years of measurements depicting the ~~diurnal-daytime~~ variability of stratospheric NO<sub>2</sub> and NO partial columns in  
15 dependence of local solar time (LST). In analogy to recently published simulation-based scaling factors by Strode et al. (2022),  
16 we created  $SF_{exp}$  normalized to ~~local solar noon~~  $SZA = 72^\circ$  for NO<sub>2</sub> and NO for every month of the year as a function of solar  
17 zenith angle (SZA). ~~Beside-Apart from~~ a boundary ~~value-value~~ problem at minimum SZA values originating in averaging over  
18 different times of the month, the obtained scaling factors  $SF_{exp}(NO_2)$  and  $SF_{exp}(NO)$  in dependence of SZA represent very well  
19 the ~~diurnaldaytime~~ behavior already shown in model simulations and experiments in the literature. This behavior is a well  
20 pronounced increase of the NO<sub>2</sub> and NO stratospheric partial column with the time of the day and a flattening of this increase  
21 after noon. In addition to the discussion of  $SF_{exp}$ , we validate the simulation-based scaling factors  $SF_{sim}(NO_2)$  (Strode et al.,  
22 2022) and present simulation-based scaling factors for NO  $SF_{sim}(NO)$ . The simulation-based scaling factors show an excellent  
23 agreement with ~~our~~ the experiment-based ones, i.e. for NO<sub>2</sub> and NO the mean ~~bias-value~~ of the modulus between experiment  
24 and simulation over all SZA and months is only 0.02 %. We show that recently used model simulations can describe very  
25 well the real behavior of nitrogen oxide (NO<sub>x</sub>) variability in the stratosphere. Furthermore, we conclude that ground-based  
26 FTIR measurements can be used for validation of the output of photochemistry models as well as creating experiment-based  
27 data sets describing the ~~diurnaldaytime~~ stratospheric NO<sub>x</sub> variability in dependence of SZA. This is a contribution to improved  
28 satellite validation and a better understanding of stratospheric photochemistry.

29

## 30 1 Introduction

31 The important role of NO<sub>2</sub> and NO in stratospheric photochemistry has been known for half a century (Crutzen, 1979). Both  
32 nitrogen oxides (NO<sub>x</sub>) are a product of the photolysis of N<sub>2</sub>O and are an important part of the ozone (O<sub>3</sub>)-destroying nitrogen  
33 catalytic cycle which controls the O<sub>3</sub> abundance in the stratosphere (Johnston, 1992). Additionally, industry and transportation  
34 are major sources of tropospheric NO<sub>x</sub>. NO<sub>x</sub> is a product of industry and traffic in the troposphere (Grewe et al., 2001).  
35 Especially in urban areas, it can serve as a precursor for e.g. O<sub>3</sub> or nitric acid (HNO<sub>3</sub>) and therefore promote smog events and  
36 directly affect human health (World Health Organization. Regional Office for Europe, 2003). Furthermore, NO<sub>2</sub> has the  
37 potential to cause significant radiative forcing during pollution events with highly elevated NO<sub>2</sub> concentrations in the  
38 troposphere (Solomon et al., 1999).

39 The monitoring and quantification of NO<sub>x</sub> total columns has been conducted since 1967 via different satellite missions (Godin-  
40 Beekmann, 2010; Rusch, 1973). For the observation of tropospheric pollution events (e.g. smog), therefore, the knowledge of  
41 the stratospheric contribution to the total column is crucial. One way to face this problem is the reference sector method, taking  
42 unpolluted total columns at a similar latitude (e.g. above the ocean) as a reference and subtract it from the total column (Richter  
43 and Burrows, 2002). The two main assumptions justifying this approach are the longitudinal homogeneity of the stratospheric  
44 column and negligible tropospheric columns over the ocean. However, due to the strong diurnal cycle of NO<sub>2</sub> and NO no time  
45 mismatch should occur between both columns.

46 One method for dealing with-to face the problem of time and site mismatches when comparing different NO<sub>x</sub> columns is the  
47 use of ground-based Fourier-transform infrared (FTIR) measurements. This method can provide data from any time of the day  
48 during sun light hours, giving the opportunity to describe diurnal/daytime NO<sub>x</sub> variabilities with a high precision, as done for  
49 NO<sub>2</sub> by Sussmann et al. (2005). For the first time, they found a reliable diurnal/daytime NO<sub>2</sub> increasing rate of  
50  $(1.02 \pm 0.12) \cdot 10^{14} \text{ cm}^{-2} \text{ h}^{-1}$  derived from FTIR measurements at mid-latitudes. Additionally, the retrieved FTIR data can have a  
51 certain altitude resolution, which allows conclusions about NO<sub>x</sub> partial column variabilities, e.g. of the stratospheric columns  
52 (Zhou et al., 2021; Yin et al., 2019). In Part I of our two companion papers (Nürnberg et al., 2023) we used these advantages  
53 of ground-based FTIR measurements to retrieve stratospheric partial columns from long-term NO<sub>2</sub> and NO measurements  
54 above Zugspitze (47.42° N, 10.98° E, 2964 m a.s.l.), Germany, yielding information on NO<sub>x</sub> diurnal/daytime variability for  
55 every month of the year. This specific data set has the potential to improve satellite validation and can serve as a basis for the  
56 description of stratospheric NO<sub>x</sub> variabilities with high time resolution. However, the data from ground-based measurements  
57 can only be received-retrieved for the limited number and locations of existing sites.

58 A method without this site restriction describing stratospheric NO<sub>x</sub> concentrations with global coverage is the use of model  
59 data from three-dimensional global transport and photochemistry models. The latter are able to describe trace gas  
60 concentrations in dependence of altitude, latitude and longitude with a very good time resolution. In comparison to one-  
61 dimensional models describing only the vertical distribution of atmospheric trace gases (e.g. O<sub>3</sub>, NO<sub>2</sub>, NO) (Allen et al., 1984;  
62 Prather and Jaffe, 1990), three-dimensional models simulate transport fluxes in all three dimensions and are able to include  
63 nearly all feedback mechanisms of the real world (Mclinden et al., 2000; Chang and Duewer, 1979). Both types of models can  
64 account for diurnal/daytime variabilities and have been used in the last decades for inter-satellite comparisons (Brohede et al.,  
65 2007; Dubé et al., 2020) as well as for satellite data validation (Bracher et al., 2005) and correction (Dubé et al., 2021; Wang  
66 et al., 2020). However, these studies differ from case to case and do not provide general global information about NO<sub>x</sub>  
67 variability. These global information should be site independent and can be applied to any satellite validation or correction all  
68 over the planet.

69 Here, a recent study of Strode et al. (2022) closed this lack-gap by developing a set of simulation-based scaling factors ( $SF_{\text{sim}}$ ),  
70 which describe the diurnal/daytime variability of NO<sub>2</sub>. A given  $SF_{\text{sim}}$  is a measure for the change of trace gas concentrations  
71 during the day normed/normalized to a specific time (here sunrise or sunset).  $SF_{\text{sim}}$  are extracted from a three-dimensional  
72 model, which considers long-range transport, stratospheric and tropospheric chemistry as well as aerosol, radiation and

Formatiert: Tiefgestellt

73 transport. The generated monthly output is available for latitudes between  $-90^\circ$  and  $90^\circ$  ( $1^\circ$  steps) and altitudes between 6 km  
74 and 78 km (0.5 km steps) for every time of the day given in solar zenith angle (SZA) values (Strode et al., 2022). This extensive  
75 research opens up the opportunity for the comparison, validation, and correction of remote and ground-based data products,  
76 by overcoming time or site mismatches.

77 However, an observational counterpart, i.e. an analogous data set of experiment-based scaling factors describing the  
78 ~~diurnal/daytime~~ increase of stratospheric  $\text{NO}_x$  still does not exist, due to the lack of reliable long-term data comprising the full  
79 ~~diurnal/daytime~~  $\text{NO}_2$  and  $\text{NO}$  variability. To close this ~~lack/gap~~, in this paper we create a set of experiment-based scaling factors  
80 ( $SF_{\text{exp}}$ ) in analogy to the simulation-based scaling factors published by Strode et al. (2002). On the one hand, this data set  
81 should serve as a general set of data describing the  $\text{NO}_x$  ~~diurnal/daytime~~ variability in dependence of SZA for the given latitude  
82 ( $47^\circ$  N) of our observation site. On the other hand, we would like to use it to validate the recently published model data for  
83  $SF_{\text{sim}}(\text{NO}_2)$  (Strode et al., 2022) as well as validate unpublished model data for  $SF_{\text{sim}}(\text{NO})$  (Sarah Strode, personal  
84 communication, 2023). For this  $SF_{\text{exp}}$  data set we will use the observational results described in Part 1 of our set of two  
85 companion papers (Nürnberg et al., 2023), where a reliable long-term data set of  $\text{NO}_2$  and  $\text{NO}$  partial columns above 16 km  
86 altitude above Zugspitze was created. As described above, these long-term data are retrieved from ground-based FTIR  
87 measurements and describe the ~~diurnal/daytime~~ variability of stratospheric  $\text{NO}_x$  within timesteps of minutes for every month  
88 of the year. ~~The cut-off point at 16 km was chosen to avoid influences of variabilities near the tropopause and in the boundary~~  
89 ~~layer upon the stratospheric partial column. Details are discussed in part 1. It is worth to mention, that~~ ~~It is outside the scope~~  
90 ~~of this work to describe with  $SF_{\text{exp}}$  the strong and fast photochemistry at sunrise and sunset.~~

91 This paper (as Part 2 of our two companion papers) briefly describes in Sect. 2 the experimental set up and the resulting FTIR  
92 data taken from Part 1 (Nürnberg et al., 2023). In Sect. 3, the dependence on SZA for  $\text{NO}_2$  and  $\text{NO}$  is shown and the resulting  
93 ~~diurnal/daytime~~ variations presented in detail in Part 1 are discussed shortly, before the  $\text{NO}_x$  partial columns ( $> 16$  km) are  
94 converted into experiment-based scaling factors ( $SF_{\text{exp}}(\text{NO}_2)$  and  $SF_{\text{exp}}(\text{NO})$ ) in Sect. 4. Finally, the resulting  $SF_{\text{exp}}$   
95 are compared qualitatively and quantitatively to  $SF_{\text{sim}}$  retrieved from model simulations.

## 96 ~~Used~~ FTIR data

97 All data of this study are retrieved from long-term ground-based FTIR solar absorption measurements at ~~the~~ Zugspitze,  
98 Germany ( $47.42^\circ$  N,  $10.98^\circ$  E, 2964 m a.s.l.). The high-altitude observatory at Zugspitze is located in the German alps and can  
99 be considered as a clean site without strong influences from pollution events in the boundary layer. The used Bruker IFS  
100 125HR spectrometer ~~is~~ ~~has~~ operated continuously since 1995 at the Zugspitze. The experimental set-up and retrieval strategy  
101 are described in our part ~~1H~~ companion paper (Nürnberg et al., 2023). ~~As described in part 1, we used daily pressure and~~  
102 ~~temperature profiles from the National Centers for Environmental Prediction (NCEP) interpolated to the measurement time.~~  
103 ~~The temperature dependency of the data cannot be discussed in detail here, but it is very likely that the stratospheric temperature~~  
104 ~~affects the  $\text{NO}_x$  concentration and therefore also the observed diurnal cycle.~~ The pollution filtered  $\text{NO}$  and  $\text{NO}_2$  stratospheric  
105 partial columns (above 16 km altitude) derived in our part ~~1H~~ study serve as a basis for the experiment-based scaling factors  
106 created now in this part ~~2H~~ work. The data set comprises 6,213  $\text{NO}$  and 16,023  $\text{NO}_2$  partial columns measured at the Zugspitze  
107 between 1995 and 2022.

## 108 3 Experimental data

### 109 3.1 $\text{NO}_x$ stratospheric partial column dependence on SZA

110 Figure 1 shows the  $\text{NO}_2$  stratospheric partial columns (black symbols) taken from Nürnberg et al. (2023) for every month as a  
111 function of SZA. Note this is the same data as shown in our Part 1 (Fig. 3 therein), which had been therein plotted as a function

Formatiert: Tiefgestellt

112 of local solar time. The  $x$ -axis is interrupted for SZA values ~~not existing without observations~~ in the respective month. Here,  
113 we define SZA to be positive in the morning from sunrise (SZA = 90°) to local solar noon (respective minimum value  
114 dependent of the season) and to be negative in the afternoon between local solar noon and sunset (SZA = -90°).

115 As already described and discussed in Part 1 of the two companion papers, the ~~diurnal daytime~~ increase of the NO<sub>2</sub> stratospheric  
116 partial column follows for every month a linear behavior from sunrise to sunset. Briefly, this behavior reflects the photolysis  
117 of the reservoir species HNO<sub>3</sub> and N<sub>2</sub>O<sub>5</sub> resulting in a consecutive increase of NO<sub>2</sub> during daytime (Crutzen, 1970).

118 Figure 2 shows in a similar way the NO stratospheric partial columns (black symbols) taken from the same work for every  
119 month in dependence of SZA (Nürnberg et al., 2023). Note this is the same data as shown in our Part 1 (Fig. 5 therein) as a  
120 function of local solar time. Briefly, the data show the typical ~~diurnal daytime~~ increase of stratospheric NO described in  
121 the literature via model calculations (Dubé et al., 2020; McLinden et al., 2000) or shown experimentally (Zhou et al., 2021; Rinsland  
122 et al., 1984) for every month. Here, the photolysis of the reservoir species N<sub>2</sub>O leads to a well-pronounced increase of  
123 stratospheric NO concentration in the morning (Crutzen, 1970). After local solar noon, the shift of the NO<sub>2</sub>-NO equilibrium,  
124 the increasing amount of O<sub>3</sub> and the solar elevation dependency of the involved photochemical reaction lead to a strong  
125 flattening of the ~~diurnal daytime~~ NO curve in dependence of SZA in comparison to NO<sub>2</sub>. This afternoon-effect is more  
126 pronounced in the summertime (mid row) than the rest of the year (Nürnberg et al., 2023).

#### 127 4 Calculation of experiment-based scaling factors

128 A set of experiment-based scaling factors ( $SF_{\text{exp}}$ ) ~~in analogy~~ to the model-based scaling factors ( $SF_{\text{sim}}$ ) published by Strode  
129 et al. (2022) was created as follows: The mean values for 2° bins of SZA of the stratospheric partial column (> 16 km) were  
130 calculated. In a next step, these mean values were normalized to ~~the minimum SZA = 72° at month 15<sup>th</sup>~~ resulting in monthly  
131  $SF_{\text{exp}}$  sets for NO<sub>2</sub> and NO shown in Fig. 3 and Fig. 4, respectively. ~~The (differing) SZAs used for normalization for the~~  
132 ~~individual months can be found in the respective legends. They are the minimum SZA at day 15 of the respective month.~~ These  
133 data reflect the ~~diurnal daytime~~ variation of stratospheric NO<sub>2</sub> and NO above Zugspitze, Germany. Values resulting from only  
134 one measurement point are shown in red without error bar.

135  $SF_{\text{exp}}(\text{NO}_2)$  (Figure 3, black and orange symbols) ~~follows every month a linear diurnal trend~~ ~~increases linearly throughout the~~  
136 ~~day in each month~~, reflecting the increase in stratospheric NO<sub>2</sub> concentration. There are two observations which can be pointed  
137 out here. First, the error bars in Fig. 3 (i.e.  $\pm 2$  standard errors of the mean,  $\pm 2 \text{ SEM} = \pm 2 \sigma / \sqrt{n}$ ) are independent of the season  
138 and are very small, reflecting a low scattering within the 2° SZA bins and enough averaging data points  $n$ . Second, in spring  
139 and autumn, at local solar noon (minimum SZA), a significant increase in  $SF_{\text{exp}}(\text{NO}_2)$  is visible. This effect can be understood  
140 as a boundary ~~value value~~ problem being due to the relatively fast change of SZA and of the NO<sub>2</sub> stratospheric partial column  
141 (seasonal variation) during the spring and autumn months, respectively. Here, the combination of both, the SZA and  
142 stratospheric partial column changes within one month end up with an increased averaged NO<sub>2</sub> stratospheric partial column  
143 near the minimum SZA. The reason is that for SZA values below the minimum SZA ~~at day 15 of each month of each month~~  
144 ~~15<sup>th</sup>~~, only partial columns from one half of the month can contribute to the average. Unfortunately, the stratospheric partial  
145 columns of this half deviate significantly from the monthly mean. Figure S1 in the supporting material illustrates this  
146 phenomenon using the NO<sub>2</sub> partial column above 16 km altitude. Here, the first half (red symbols) and the second half (blue  
147 symbols) of April is split up into two datasets underlining the described boundary ~~layer value~~ problem. At low SZA values,  
148 only blue data points sum up to the averaged values, considering only the second half of the month. Consequently, the partial  
149 column and of course the scaling factor increases artificially ~~(pointed out by the blue arrow in the figure)~~. This effect leads us  
150 to the exclusion of these data points (Figure 3, orange symbols) below the minimum SZA reached at day 15 of the respective  
151 month. ~~Another opportunity to face this problem would be the choice of a smaller time binning (e.g. 2 weeks, 10 days).~~

152 However, this would i) worsen the comparability to the simulation-based scaling factors and ii) reduce the usable data base  
153 per time bin. The whole used data set of  $SF_{\text{exp}}(\text{NO}_2)$  can be found in the supporting material Table S1-S4.

154 For  $SF_{\text{exp}}(\text{NO})$  (Figure 4, black and orange symbols), the difference in ~~diurnal/daytime~~ increase in comparison to  $\text{NO}_2$  is very  
155 well pronounced. Before local solar noon,  $SF_{\text{exp}}$  increases for every month linearly. After local solar noon, the described  
156 flattening of the increase is visible. Here, the NO stratospheric partial column stays almost constant within the scattering until  
157 sunset independent of the season. The  $\pm 2$  SEM error bars of  $SF_{\text{exp}}(\text{NO})$  shown in Fig. 4 are also very small, but more values  
158 are excluded (red symbols) due to the availability of only one measurement point within the corresponding  $2^\circ$  SZA bin. This  
159 reflects the lower data base of the NO retrieval, originated in the use of another spectral micro-window for analysis. However,  
160 the small error bars underline, that for most of the mean values, the data base is reliable. Near local solar noon for  $SF_{\text{exp}}(\text{NO})$   
161 a similar but even less pronounced effect can be seen, as described for  $\text{NO}_2$ -before. Here, the deviation from the visible trend  
162 at spring or autumn months is very small. However, for consistent data handling we will also exclude the respective values  
163 (orange symbols) for  $SF_{\text{exp}}(\text{NO})$  below the minimum SZA at each month 15<sup>th</sup>. The whole used data set of  $SF_{\text{exp}}(\text{NO})$  can be  
164 found in the supporting material Table S5-S8.

## 165 5 Model comparison of $\text{NO}_x$ scaling factors

166 In the previous section, we created experiment-based averaged monthly scaling factors  $SF_{\text{exp}}$  for  $\text{NO}_2$  and NO describing the  
167 ~~diurnal/daytime~~ variation of stratospheric  $\text{NO}_x$  concentration above Zugspitze, Germany. Next, we will compare the discussed  
168 results for  $SF_{\text{exp}}$  to model-based scaling factors  $SF_{\text{sim}}$  for  $\text{NO}_2$  published by Strode et al. (2022) and for NO calculated from the  
169 same GEOS-GMI model simulation as the  $\text{NO}_2$  scaling factors. Details of the GEOS model simulation with GMI chemistry  
170 (Duncan et al., 2007; Strahan et al., 2007; Nielsen et al., 2017) are described in Strode et al. (2022) and refs therein. The model  
171 parameters and the analysis method can be found in the literature (Strode et al., 2022). The given scaling factors  $SF_{\text{sim}}(\text{NO}_2)$   
172 and  $SF_{\text{sim}}(\text{NO})$  are available for 146 levels between 6 km and 78.5 km altitude in a 0.5 km grid and are ~~normed~~normalized to  
173  $\text{SZA} = 90^\circ$  (sunrise). For a better comparison of experiment and model, we calculated mean values for  $SF_{\text{sim}}$  which also  
174 represent the stratospheric partial column above 16 km altitude. In order to do so, for each model level  $z$ ,  $SF_{\text{sim}}(z)$  was weighted  
175 to the mean monthly partial column profile of the given  $\text{NO}_x$  retrieval at  $z$  and  $SF_{\text{sim}}(> 16 \text{ km})$  was obtained via averaging over  
176  $SF_{\text{sim}}(16 \text{ km})$  to  $SF_{\text{sim}}(78.5 \text{ km})$ . Furthermore,  $SF_{\text{sim}}(> 16 \text{ km})$  was ~~also-normalized to the minimum~~  $\text{SZA} = 72^\circ$  (rather than  
177 sunrise/sunset) ~~at month 15<sup>th</sup>~~ as done for  $SF_{\text{exp}}$  in Sect. 4.

178  $SF_{\text{sim}}(\text{NO}_2)$  and  $SF_{\text{sim}}(\text{NO})$  are additionally shown in Fig. 5 and Fig. 6, respectively (red line). At first appearance,  $SF_{\text{exp}}$  (black  
179 symbols) and  $SF_{\text{sim}}$  (red line) fits together very well and the model data follow the experimental ~~diurnal/daytime~~ variation for  
180 both species  $\text{NO}_2$  and NO.

### 181 5.1.1 Quantitative evaluation

182 For the quantitative evaluation of the model comparison, the residuals between experiment and model  $(SF_{\text{exp}} - SF_{\text{sim}})/SF_{\text{sim}}$  are  
183 calculated for  $SF(\text{NO}_2)$  and  $SF(\text{NO})$  and are shown in Fig. 7 and Fig. 8, respectively. Additionally, the mean bias per month is  
184 shown as a mean value over all SZA (red dotted line).

185 The residuals of  $SF(\text{NO}_2)$  (Figure 7) show over the whole ~~season-year~~ a very good agreement between experiment and model  
186 within  $\pm 0.2\%$ , reflecting the high quality of the GEOS GMI simulation at midlatitudes. Only for a few months, significant  
187 differences between experiment and model are visible ~~at high SZA values (near sunrise)~~. For ~~April, August, and~~ September  
188 ~~and October~~, the morning increase of  $\text{NO}_2$  is less pronounced in the model, leading to a significant deviation from the  
189 experimental values and an ~~overestimation-underestimation~~ of the experiment-based scaling factors  $SF_{\text{exp}}$  ~~at noon~~. However,  
190 the experimental values describing the stratospheric  $\text{NO}_2$  variability can be also influenced by tropospheric variations, because  
191 the used  $\text{NO}_2$  partial column cannot be treated as completely independent of the tropospheric partial column (see Nürnberg et

192 al. (2023)). Furthermore, the model data offer higher uncertainties during twilight which can lead to deviations from  
193 experiment (Alvanos and Christoudias, 2019).

194 Table 1 shows the mean bias (see also Figure 7, red dotted line) for every month calculated from the residuals shown in  
195 Fig. 7 together with two times the SEM ( $2 \sigma/\sqrt{n}$ ). Unfortunately, due to the small values of 2 SEM of 0.006563 % to  
196 0.01923 % for most of the months (except ~~January, March, July, October, November, February, Jun and December~~), 2 SEM is  
197 smaller than the mean bias. Therefore, when taking 2 SEM as a quantitative indicator,  $SF_{exp}$  and  $SF_{sim}$  agrees only in four  
198 months within the margin of error. However, when considering the mean deviation between experiment and model of below  
199 |0.068444 %| per month, we can state that the model data published by Strode et al. (2022) reflect sufficiently well the  
200 experimental values retrieved from solar FTIR measurements at midlatitudes.

201 A very similar behavior can be obtained for  $SF(NO)$  (Figure 8). With a maximum deviation of  $\pm 0.2$  % the agreement between  
202 experiment and model is very similar as seen for  $NO_2$ . However, it is remarkable, that for the specific-months with highest  
203 SZA (January, February, ~~August, June, September, October, December~~) the first last-data points after nearest to sunrise for  
204 which measurements exist (high SZA region) deviate significantly from zero. Comparing to Fig. 6, the experimental values in  
205 this region seems not to follow the continuous increase expected from model descriptions. Here, an error source of the  
206 experimental data can be the wide range in photochemical regimes along the line-of-sight of the FTIR slant column  
207 measurements at high SZA: high up in the atmosphere, the sun is already well above the horizon, so  $NO_2$  production less has  
208 been significant already, while lower down the atmosphere is still much darker and  $NO_2$  levels still lower/higher. The FTIR  
209 retrieval leads to an averaging over these effects because from the solar measurements  $NO_2$  slant columns along the line of  
210 sight are retrieved, and these are then converted to vertical column densities using a simple  $\cos(SZA)$  airmass correction.

211 Furthermore, the  $NO$  increase in the morning is more pronounced in the model, leading to a significant deviation from the  
212 experimental values and an underestimation/overestimation of the experiment-based scaling factors  $SF_{exp}$  at noon. In the same  
213 manner as discussed before for  $NO_2$ , the experimental values describing the stratospheric  $NO$  variability can be influenced by  
214 tropospheric variations, because the used  $NO$  partial column cannot be treated as completely independent of the tropospheric  
215 partial column (see Nürnberg et al. (2023)). Consequently, the lower stratospheric partial column in the morning is more  
216 influenced by the tropospheric partial column than in the evening.

217 In the same way as done for  $NO_2$ , the mean bias (see also Fig. 8, red dotted line) and  $2 \sigma/\sqrt{n}$  (2 SEM) are calculated and are  
218 shown in Table 2 for the  $NO$  residuals. Here, a better agreement between experiment and model can be quantified. For  
219 ~~seven~~ six months (January, ~~February, June, September, October, November, December, March, April, May, November,~~  
220 ~~December~~) the mean bias is smaller than 2 SEM indicating an agreement between experiment and model within the error bars.  
221 Nevertheless, this observation not only reflects a better agreement between experiment and model but can be also explained  
222 with a higher scattering of the residuals leading to a higher SEM. This can be confirmed when comparing the values for 2 SEM  
223 given in Table 1 and Table 2. With a mean 2 SEM of the residuals over all months of 0.00963 % for  $NO_2$  and  
224 0.018594 % for  $NO$ , respectively, the residual scattering with a similar  $n$  and a similar mean bias of 0.02 % is two times larger  
225 for  $NO$ .

226 In conclusion, the quantitative comparison of the experimental derived scaling factors  $SF_{exp}$  and the scaling factors derived  
227 from model simulations  $SF_{sim}$  for  $NO_2$  and  $NO$  showed very good agreement of both data sets with a mean bias between  
228 experiment and model of only 0.02 % over all months underlining the quality of the model data at midlatitudes and the  
229 reliability of the retrieved experiment-based scaling factors.

## 6 Summary and Conclusions

In this work, we reanalyzed an experimental long-term data set from solar FTIR measurements over 25 years of measurement at the Zugspitze (47.42° N, 10.98° E, 2964 m a.s.l.), Germany, published ~~along~~ in a companion paper (Part 1, Nürnberg et al., 2023). We present for the first time experiment-based scaling factors  $SF_{\text{exp}}$  in dependence of the solar zenith angle (SZA) representing monthly ~~diurnal~~~~daytime~~  $\text{NO}_2$  and  $\text{NO}$  variabilities in the stratosphere (> 16 km altitude) within timesteps of minutes.  $SF_{\text{exp}}$  is a measure for the variability of the  $\text{NO}_x$  partial column above 16 km altitude in comparison to local solar noon. We calculated  $SF_{\text{exp}}$  from the time dependent monthly  $\text{NO}_x$  partial columns (published in Part 1) by averaging over SZA bins of 2° and a normalization to the minimum SZA at day 15 of the respective month. The resulting values of  $SF_{\text{exp}}(\text{NO}_2)$  and  $SF_{\text{exp}}(\text{NO})$  reflect very well the expected ~~diurnal~~~~daytime~~ variability of  $\text{NO}_2$  and  $\text{NO}$  described in Part 1 (Nürnberg et al., 2023). Only the boundary values in spring and autumn months deviate significantly due to the relatively fast change of the minimum SZA during these months influencing the average value. Neglecting these values leads to two reliable experiment-based data sets for  $SF_{\text{exp}}(\text{NO}_2)$  and  $SF_{\text{exp}}(\text{NO})$ . Furthermore, we used these new experiment-based data sets to validate recently ~~calculated~~ published simulation-based scaling factors  $SF_{\text{sim}}(\text{NO}_2)$  (Strode et al., 2022) and recently ~~calculated~~ simulation-based scaling factors  $SF_{\text{sim}}(\text{NO})$  from a global study representing a similar latitude (47 °N). Comparing experiment and model simulation, we find an excellent agreement for stratospheric  $\text{NO}_2$  and  $\text{NO}$  ~~diurnal~~~~daytime~~ variabilities with a mean bias of the modulus over all months and SZA of only 0.02 % with no significant deviating trends for boundary values. These results underline the quality of recent multi-dimensional model simulations of stratospheric trace gases, representing very well experimental data. Additionally, we showed, that ground-based FTIR measurements can provide reliable information about stratospheric  $\text{NO}_x$  variability within time steps of minutes, which can serve as a good basis for the validation of global model simulations and therefore can help to further optimize satellite validations.

The analysis method of the retrieval of stratospheric  $\text{NO}_2$  and  $\text{NO}$  partial columns over Zugspitze, Germany, published in Part 1 of the two companion papers (Nürnberg et al., 2023) in combination with the generalization of this data by calculating unitless scaling factors  $SF$  and the validation of recently published model data in this paper (Part 2) can be seen as a strong tool for the further validation and correction of global model and satellite data. This approach can be taken for any ground-based FTIR spectrometer generating a global set of experiment-based stratospheric  $\text{NO}_2$  and  $\text{NO}$  partial columns or scaling factors  $SF_{\text{exp}}(\text{NO}_2)$  and  $SF_{\text{exp}}(\text{NO})$ .

### Data availability

The presented calculated experimental factors  $SF_{\text{exp}}$  ~~and the used partial columns in dependent of the SZA~~ can be found in the supporting material of this paper. The used experimental data is published along in Part 1 of the two companion papers (Nürnberg et al., 2023). Any other data of interest underlying this publication can be obtained at any time from the corresponding author on demand. The simulated scaling factors for  $\text{NO}_2$  and  $\text{NO}$  are available at this website: [https://avdc.gsfc.nasa.gov/pub/data/project/GMI\\_SF/](https://avdc.gsfc.nasa.gov/pub/data/project/GMI_SF/)

### Author contributions

~~PN optimized and performed the FTIR retrievals, made the scientific analysis, and wrote the manuscript. SAS performed the model simulations and processed the data for the comparison to experiment and supported editing of the manuscript. RS suggested this research, contributed to the design of the study, and supported editing of the manuscript.~~

Formatiert: Standard



266 **Competing Interests**

267 None.

268 **Acknowledgements**

269 ~~Funding by the Federal Ministry of Education and Research of Germany within the ACTRIS-D project (grant no. 01LK2001B)~~  
270 ~~is gratefully acknowledged. We acknowledge funding by the Helmholtz Changing Earth – Sustaining our Future research~~  
271 ~~program within the Earth and Environment research field~~~~Funding by the Federal Ministry of Education and Research of~~  
272 ~~Germany within the Project ACTRIS D (grant 01LK2001B) is gratefully acknowledged. We acknowledge funding by the~~  
273 ~~Helmholtz Research Program “Changing Earth—Sustaining our Future” within the Research Field “Earth and Environment”~~  
274 ~~and by the KIT Publication Fund of the Karlsruhe Institute of Technology.~~ SAS acknowledges support from NASA grant  
275 80NSSC18K0711, the NASA Modeling, Analysis, and Prediction (MAP) Program, and computing resources from the NASA  
276 Center for Climate Simulation (NCCS) for the simulated scaling factors.  
277

- Allen, M., Lunine, J. I., and Yung, Y. L.: The vertical distribution of ozone in the mesosphere and lower thermosphere, *Journal of Geophysical Research*, 89, 4841-4872, doi: 10.1029/JD089iD03p04841, 1984.
- Alvanos, M. and Christoudias, T.: Accelerating Atmospheric Chemical Kinetics for Climate Simulations, *IEEE Transactions on Parallel and Distributed Systems*, 30, 2396-2407, doi: 10.1109/TPDS.2019.2918798, 2019.
- Bracher, A., Sinnhuber, M., Rozanov, A., and Burrows, J. P.: Using a photochemical model for the validation of NO<sub>2</sub> satellite measurements at different solar zenith angles, *Atmospheric Chemistry and Physics*, 5, 393-408, doi: 10.5194/acp-5-393-2005, 2005.
- Brohede, S. M., Haley, C. S., McLinden, C. A., Sioris, C. E., Murtagh, D. P., Petelina, S. V., Llewellyn, E. J., Bazureau, A., Goutail, F., Randall, C. E., Lumpe, J. D., Taha, G., Thomasson, L. W., and Gordley, L. L.: Validation of Odin/OSIRIS stratospheric NO<sub>2</sub> profiles, *Journal of Geophysical Research: Atmospheres*, 112, doi: 10.1029/2006JD007586, 2007.
- Chang, J. and Duewer, W. H.: Modeling chemical processes in the stratosphere, *Annual Review of Physical Chemistry*, 30, 443-469, 1979.
- Crutzen, P. J.: The influence of nitrogen oxides on the atmospheric ozone content, *Quarterly Journal of the Royal Meteorological Society*, 96, 320-325, doi: 10.1002/qj.49709640815, 1970.
- Crutzen, P. J.: The Role of NO and NO<sub>2</sub> in the Chemistry of the Troposphere and Stratosphere, *Annual Review of Earth and Planetary Sciences*, 7, 443-472, doi: 10.1146/annurev.ea.07.050179.002303, 1979.
- Dubé, K., Randel, W., Bourassa, A., Zawada, D., McLinden, C., and Degenstein, D.: Trends and Variability in Stratospheric NO<sub>x</sub> Derived From Merged SAGE II and OSIRIS Satellite Observations, *Journal of Geophysical Research: Atmospheres*, 125, doi: 10.1029/2019jd031798, 2020.
- Dubé, K., Bourassa, A., Zawada, D., Degenstein, D., Damadeo, R., Flittner, D., and Randel, W.: Accounting for the photochemical variation in stratospheric NO<sub>2</sub> in the SAGE III/ISS solar occultation retrieval, *Atmospheric Measurement Techniques*, 14, 557-566, doi: 10.5194/amt-14-557-2021, 2021.
- Duncan, B. N., Strahan, S. E., Yoshida, Y., Steenrod, S. D., and Livesey, N.: Model study of the cross-tropopause transport of biomass burning pollution, *Atmospheric Chemistry and Physics*, 7, 3713-3736, doi: 10.5194/acp-7-3713-2007, 2007.
- Godin-Beekmann, S.: Spatial observation of the ozone layer, *Comptes Rendus Geoscience*, 342, 339-348, doi: 10.1016/j.crte.2009.10.012, 2010.
- Grewe, V., Brunner, D., Dameris, M., Grenfell, J. L., Hein, R., Shindell, D., and Staehelin, J.: Origin and variability of upper tropospheric nitrogen oxides and ozone at northern mid-latitudes, *Atmospheric Environment*, 35, 3421-3433, doi: 10.1016/s1352-2310(01)00134-0, 2001.
- Johnston, H. S.: Atmospheric ozone, *Annu Rev Phys Chem*, 43, 1-31, doi: 10.1146/annurev.pc.43.100192.000245, 1992.
- McLinden, C. A., Olsen, S. C., Hannegan, B., Wild, O., Prather, M. J., and Sundet, J.: Stratospheric ozone in 3-D models: A simple chemistry and the cross-tropopause flux, *Journal of Geophysical Research: Atmospheres*, 105, 14653-14665, doi: 10.1029/2000jd900124, 2000.
- Nielsen, J. E., Pawson, S., Molod, A., Auer, B., da Silva, A. M., Douglass, A. R., Duncan, B., Liang, Q., Manyin, M., Oman, L. D., Putman, W., Strahan, S. E., and Wargan, K.: Chemical Mechanisms and Their Applications in the Goddard Earth Observing System (GEOS) Earth System Model, *J Adv Model Earth Syst*, 9, 3019-3044, doi: 10.1002/2017MS001011, 2017.
- Nürnberg, P., Sussmann, R., and Rettinger, M.: Solar FTIR measurements of NO<sub>x</sub> vertical distributions: Part I) First observational evidence for a seasonal variation in the diurnal increasing rates of stratospheric NO<sub>2</sub> and NO, *Atmos. Chem. Phys.*, 2023.
- Prather, M. and Jaffe, A. H.: Global impact of the Antarctic ozone hole: Chemical propagation, *Journal of Geophysical Research*, 95, 3473-3492, doi: 10.1029/JD095iD04p03473, 1990.
- Richter, A. and Burrows, J. P.: Tropospheric NO<sub>2</sub> from GOME measurements, *Advances in Space Research*, 29, 1673-1683, doi: 10.1016/s0273-1177(02)00100-x, 2002.
- Rinsland, C. P., Boughner, R. E., Larsen, J. C., Stokes, G. M., and Brault, J. W.: Diurnal variations of atmospheric nitric oxide: Ground-based infrared spectroscopic measurements and their interpretation with time-dependent photochemical model calculations, *Journal of Geophysical Research*, 89, 9613-9622, doi: 10.1029/JD089iD06p09613, 1984.
- Rusch, D. W.: Satellite ultraviolet measurements of nitric oxide fluorescence with a diffusive transport model, *Journal of Geophysical Research*, 78, 5676-5686, doi: 10.1029/JA078i025p05676, 1973.
- Solomon, S., Portmann, R. W., Sanders, R. W., Daniel, J. S., Madsen, W., Bartram, B., and Dutton, E. G.: On the role of nitrogen dioxide in the absorption of solar radiation, *Journal of Geophysical Research: Atmospheres*, 104, 12047-12058, doi: 10.1029/1999jd900035, 1999.
- Strahan, S. E., Duncan, B. N., and Hoor, P.: Observationally derived transport diagnostics for the lowermost stratosphere and their application to the GMI chemistry and transport model, *Atmospheric Chemistry and Physics*, 7, 2435-2445, doi: 10.5194/acp-7-2435-2007, 2007.
- Strode, S. A., Taha, G., Oman, L. D., Damadeo, R., Flittner, D., Schoeberl, M., Sioris, C. E., and Stauffer, R.: SAGE III/ISS ozone and NO<sub>2</sub> validation using diurnal scaling factors, *Atmospheric Measurement Techniques*, 15, 6145-6161, doi: 10.5194/amt-15-6145-2022, 2022.
- Sussmann, R., Stremme, W., Burrows, J. P., Richter, A., Seiler, W., and Rettinger, M.: Stratospheric and tropospheric NO<sub>2</sub> variability on the diurnal and annual scale: a combined retrieval from ENVISAT/SCIAMACHY and solar FTIR at the Permanent Ground-Truthing Facility Zugspitze/Garmisch, *Atmospheric Chemistry and Physics*, 5, 2657-2677, doi: 10.5194/acp-5-2657-2005, 2005.

Formatiert: Englisch (Vereinigte Staaten)

340 Wang, S., Li, K.-F., Zhu, D., Sander, S. P., Yung, Y. L., Pazmino, A., and Querel, R.: Solar 11-Year Cycle Signal in  
341 Stratospheric Nitrogen Dioxide—Similarities and Discrepancies Between Model and NDACC Observations, *Solar Physics*,  
342 295, 117, doi: 10.1007/s11207-020-01685-1, 2020.  
343 World Health Organization. Regional Office for Europe: Health aspects of air pollution with particulate matter, ozone and  
344 nitrogen dioxide : report on a WHO working group, Bonn, Germany 13-15 January 2003, Copenhagen : WHO Regional Office  
345 for Europe, <https://apps.who.int/iris/handle/10665/107478>, 2003.  
346 Yin, H., Sun, Y., Liu, C., Zhang, L., Lu, X., Wang, W., Shan, C., Hu, Q., Tian, Y., Zhang, C., Su, W., Zhang, H., Palm, M.,  
347 Notholt, J., and Liu, J.: FTIR time series of stratospheric NO<sub>2</sub> over Hefei, China, and comparisons with OMI and GEOS-Chem  
348 model data, *Opt Express*, 27, A1225-A1240, doi: 10.1364/OE.27.0A1225, 2019.  
349 Zhou, M., Langerock, B., Vigouroux, C., Dils, B., Hermans, C., Kumps, N., Nan, W., Metzger, J.-M., Mahieu, E., Wang, T.,  
350 Wang, P., and De Mazière, M.: Tropospheric and stratospheric NO retrieved from ground-based Fourier-transform infrared  
351 (FTIR) measurements, *Atmospheric Measurement Techniques*, 14, 6233-6247, doi: 10.5194/amt-14-6233-2021, 2021.  
352

353

Feldfunktion geändert

Formatiert: Englisch (Vereinigte Staaten)

Formatiert: Englisch (Vereinigte Staaten)

354  
355

**Table 1** Table 1. Calculated mean bias of residuals ( $[SF_{exp}-SF_{sim}]/SF_{sim}$ ) for every month between experiment and simulations for NO<sub>2</sub> and the standard error of the mean ( $\sigma/\sqrt{n}$ ) of this value.

Month	J (%)	F (%)	M (%)	A (%)	M (%)	J (%)	J (%)	A (%)	S (%)	O (%)	N (%)	D (%)
mean bias	$\frac{0.0230}{0.0065}$	$\frac{0.0257}{0.0050}$	$\frac{0.0024}{0.0438}$	$\frac{0.0433}{0.0364}$	$\frac{0.0118}{0.0071}$	$\frac{0.0683}{0.0082}$	$\frac{0.0060}{0.0194}$	$\frac{0.0207}{0.0404}$	$\frac{0.0414}{0.0280}$	$\frac{0.0062}{0.0444}$	$\frac{0.0007}{0.0407}$	$\frac{0.0204}{0.0138}$
$2\sigma/\sqrt{n}$	$\frac{0.0132}{0.0136}$	$\frac{0.0092}{0.0094}$	$\frac{0.0088}{0.0084}$	$\frac{0.0082}{0.0076}$	$\frac{0.0065}{0.0063}$	$\frac{0.0096}{0.0085}$	$\frac{0.0077}{0.0076}$	$\frac{0.0093}{0.0087}$	$\frac{0.0081}{0.0076}$	$\frac{0.0072}{0.0069}$	$\frac{0.0085}{0.0081}$	$\frac{0.0192}{0.0193}$
bias < 2SEM ?	YesNo	NoYes	NoYes	NoNo	No	YesNo	NoYes	No	No	NoYes	NoYes	NoYes

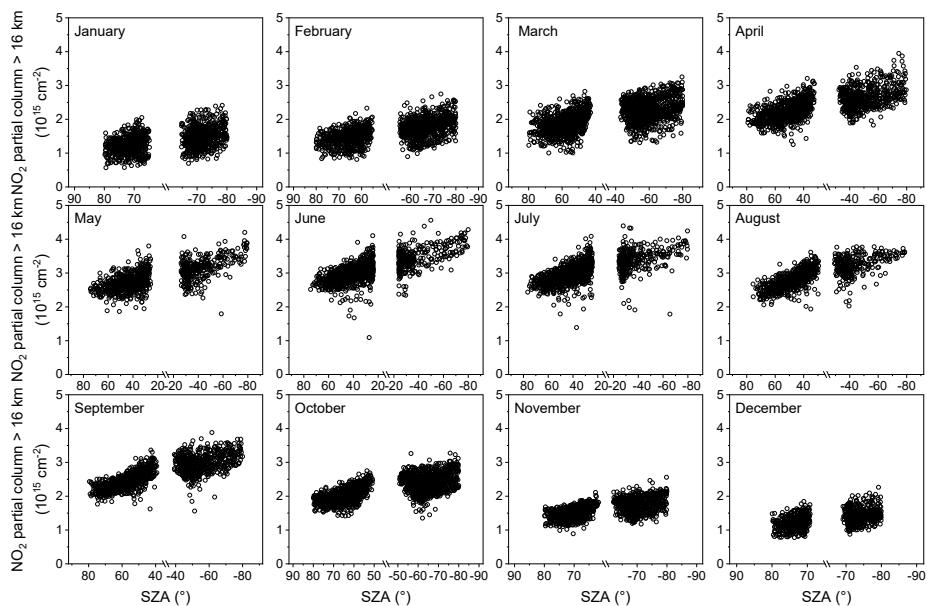
356

357  
358

**Table 2** Table 2. Calculated mean bias of residuals ( $[SF_{exp}-SF_{sim}]/SF_{sim}$ ) for every month between experiment and simulations for NO and 2 times the standard error of the mean ( $2\sigma/\sqrt{n}$ ) of this value.

Month	J (%)	F (%)	M (%)	A (%)	M (%)	J (%)	J (%)	A (%)	S (%)	O (%)	N (%)	D (%)
mean bias	$\frac{0.0045}{0.0060}$	$\frac{0.0592}{0.0126}$	$\frac{0.0220}{0.0105}$	$\frac{0.0269}{0.0028}$	$\frac{0.0714}{0.0008}$	$\frac{0.0046}{0.0164}$	$\frac{0.0889}{0.0206}$	$\frac{0.0767}{0.0397}$	$\frac{0.0068}{0.0556}$	$\frac{0.0118}{0.0316}$	$\frac{0.0096}{0.0096}$	$\frac{0.0150}{0.0150}$
$2\sigma/\sqrt{n}$	$\frac{0.0331}{0.0335}$	$\frac{0.0236}{0.0254}$	$\frac{0.0166}{0.0168}$	$\frac{0.0110}{0.0112}$	$\frac{0.0099}{0.0107}$	$\frac{0.0160}{0.0163}$	$\frac{0.0143}{0.0160}$	$\frac{0.0102}{0.0115}$	$\frac{0.0117}{0.0124}$	$\frac{0.0138}{0.0144}$	$\frac{0.0191}{0.0179}$	$\frac{0.0425}{0.0425}$
bias < 2SEM ?	YesYe	YesNo	YesNo	YesNo	YesNo	NoYes	NoNo	No	NoYes	NoYes	YesYe	Yes

359



360

361  
362

**Figure 1.** Retrieved NO<sub>2</sub> partial column above 16 km altitude measured at Zugspitze (black symbols) for every month in dependence of SZ A.

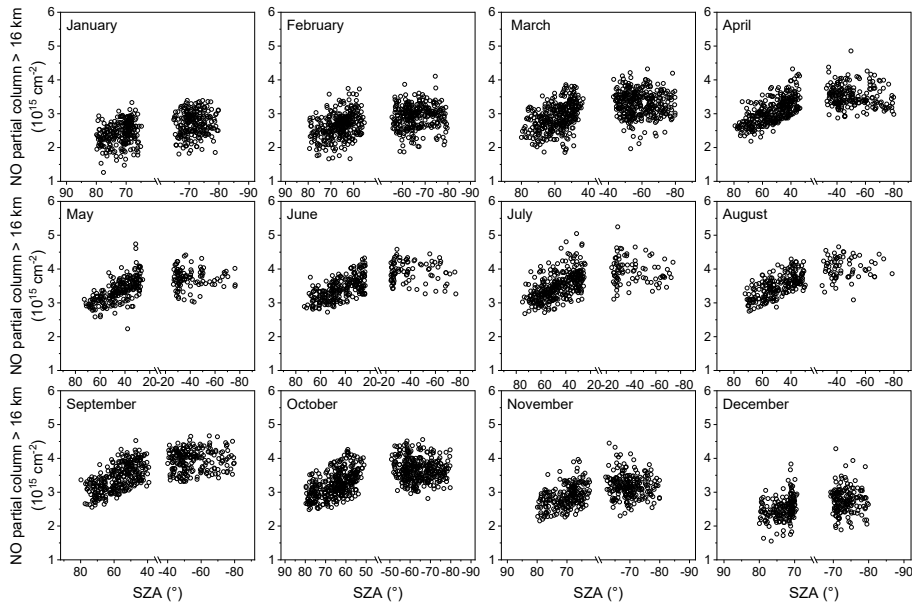
Formatiert: Vom nächsten Absatz trennen

Formatierte Tabelle

Formatiert: Vom nächsten Absatz trennen

Formatierte Tabelle

Formatierte Tabelle



363

364

**Figure 2.** Retrieved NO partial column above 16 km altitude measured at Zugspitze (black symbols) for every month in dependence of SZA.

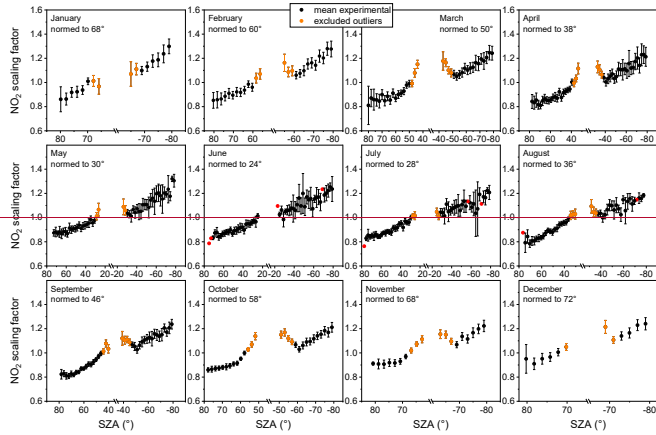
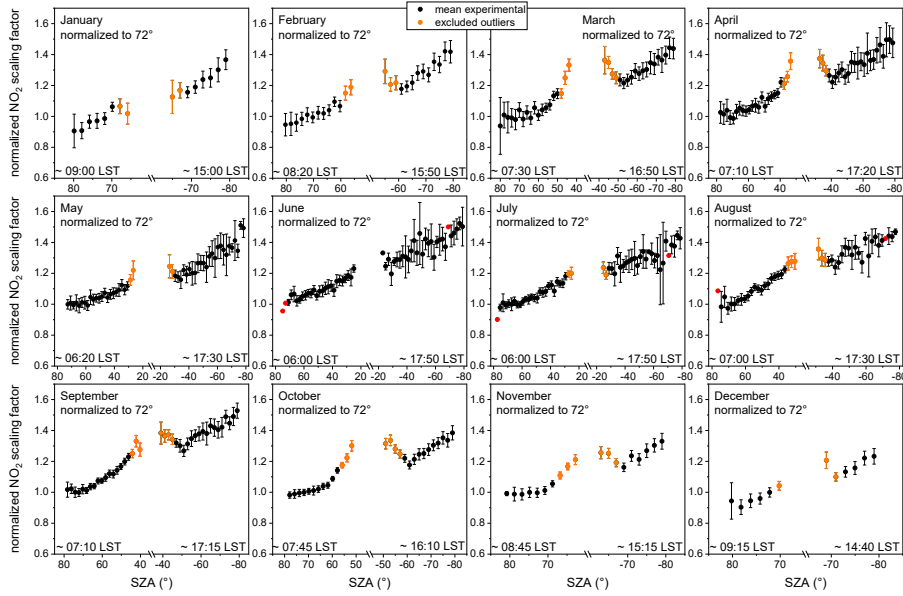
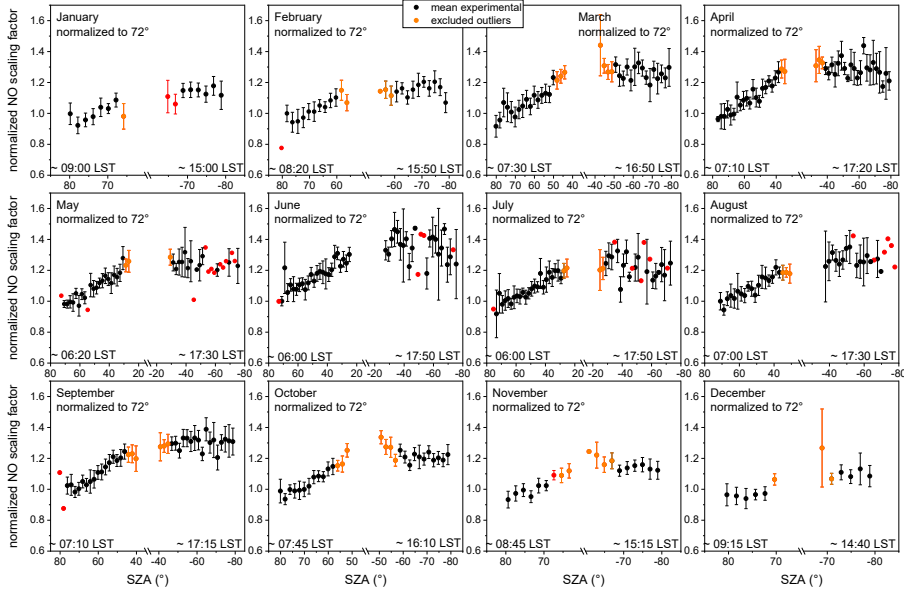
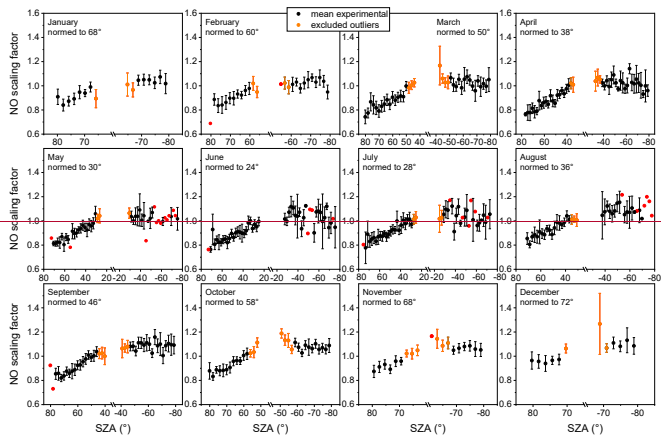


Figure 3. Calculated ~~normed~~ normalized  $NO_2$  scaling factors  $SF_{exp}(NO_2)$  above 16 km altitude measured at Zugspitze (black; orange symbols are excluded outliers) for every month in dependence of the SZA. The values represent the mean value within  $2^\circ$  SZA bins. The error bars represent two times the standard error of the mean ( $\pm 2 \sigma/\sqrt{n}$ ) value. Values resulting from only one measurement point are shown in red without error bar. ~~The SZA used for normalization for the respective month for experiment and model is given in each legend.~~



371



372

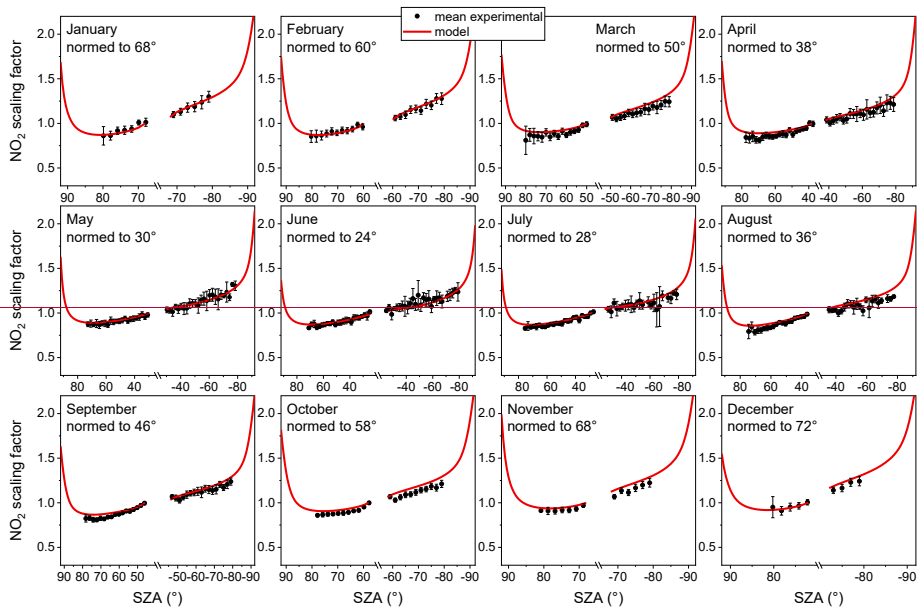
373

374

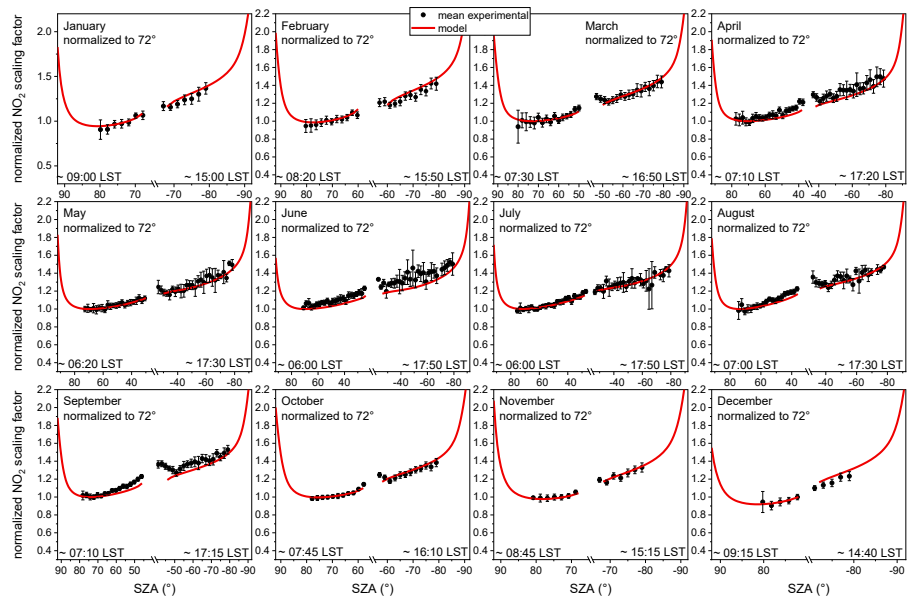
375

376

**Figure 4.** Calculated ~~normed~~normalized NO scaling factors  $SF_{exp}(NO)$  above 16 km altitude measured at Zugspitze (black; orange are excluded outliers) for every month in dependence of SZA. The values represent the mean value within  $2^\circ$  SZA bins. The error bars represent two times the standard error of the mean ( $\pm 2 \sigma/\sqrt{n}$ ) value. Values resulting from only one measurement point are shown in red without error bar. ~~The SZA used for normalization for the respective month for experiment and model is given in each legend.~~



377

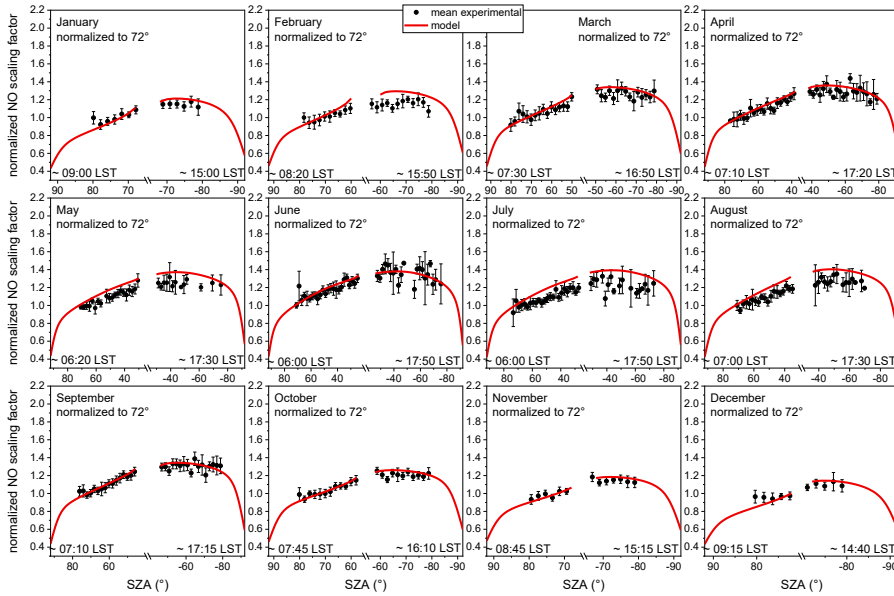


378

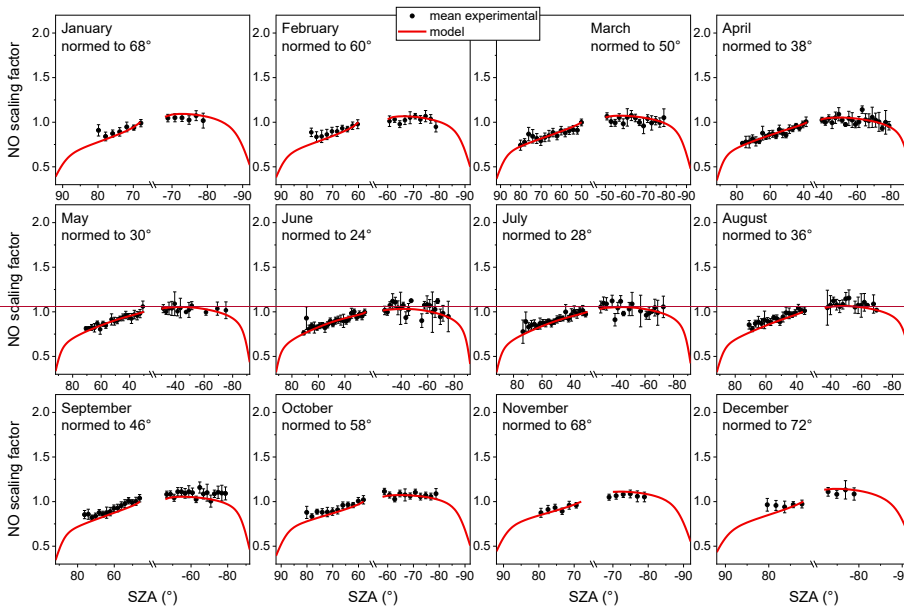
379 **Figure 5.** Calculated normednormalized  $SF_{exp}(NO_2)$  above 16 km altitude measured at Zugspitze (black) and  
 380 recalculated normednormalized  $SF_{sim}(NO_2)$  above 16 km altitude (red line) for every month in dependence of SZA. The  
 381 experimental values represent the mean value within 2° SZA bins. The error bars represent two times the standard error of the mean ( $\pm 2$   
 382  $\sigma/\sqrt{n}$ ) value. **The SZA used for normalization for the respective month for experiment and model is given in each legend.**

Feldfunktion geändert



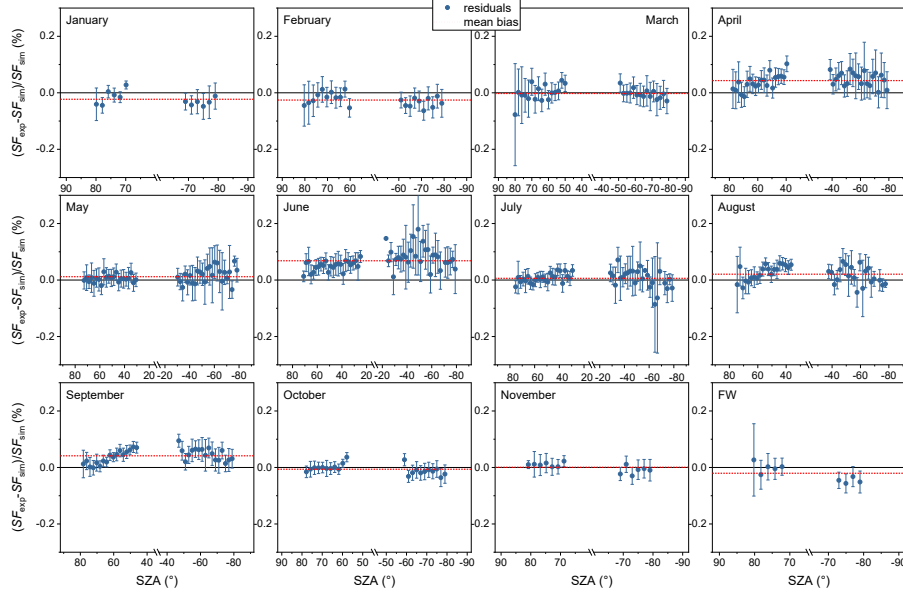


383

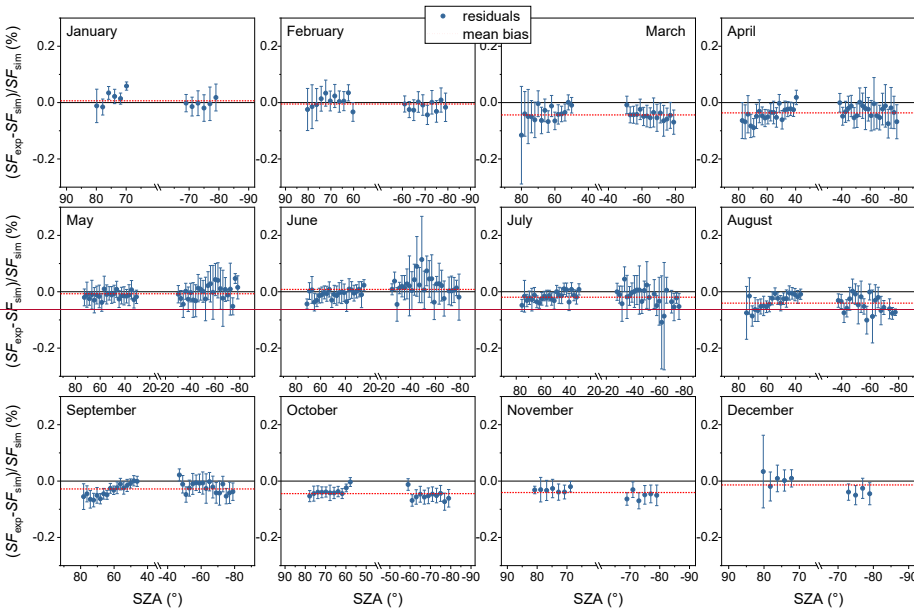


384

385 **Figure 6.** Calculated **normednormalized** NO scaling factors  $SF_{exp}(NO)$  above 16 km altitude measured at Zugspitze (black) and recalculated  
 386 **normednormalized** NO scaling factors  $SF_{sim}(NO)$  above 16 km altitude (red line) for every month in dependence of SZA. The experimental  
 387 values represent the mean value within 2° SZA bins. The error bars represent two times the standard error of the mean ( $\pm 2 \sigma/\sqrt{n}$ ) value.  
 388 **The SZA used for normalization for the respective month for experiment and model is given in each legend.**

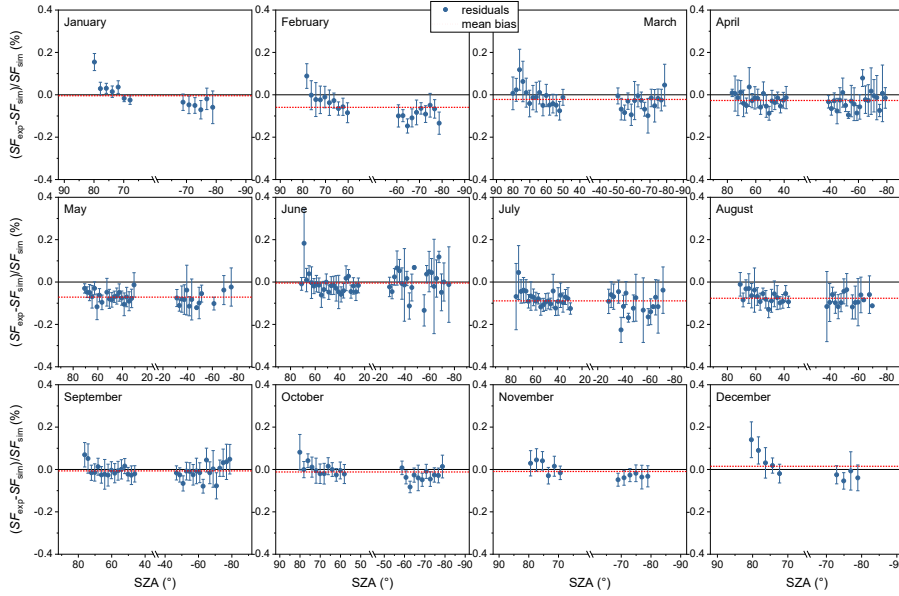


389

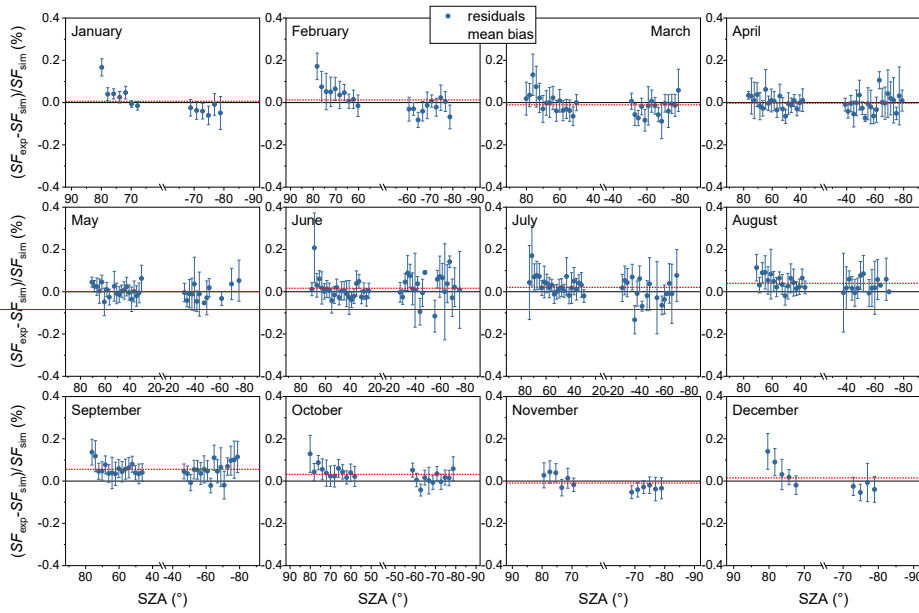


390

391 **Figure 7.** Calculated residuals  $(SF_{exp}-SF_{sim})/SF_{sim}$  between the experimental ~~normed~~ ~~normalized~~ mean NO<sub>2</sub> scaling factors  $SF_{exp}$  and the  
 392 simulated ~~normed~~ ~~normalized~~ NO<sub>2</sub> scaling factors  $SF_{sim}$  and interpolated to the respective SZA for every month in dependence of SZA. The  
 393 error bars represent two times the propagated standard error of the mean ( $\pm 2 \sigma/\sqrt{n}$ ) of the experimental value. The mean bias over all SZA  
 394 is shown in red.



395



396

397

398

399

400

**Figure 8.** Calculated residuals  $(SF_{exp}-SF_{sim})/SF_{sim}$  between the experimental ~~normed~~ normalized mean NO scaling factors  $SF_{exp}$  and the simulated ~~normed~~ normalized NO scaling factors  $SF_{sim}$  and interpolated to the respective SZA for every month in dependence of SZA. The error bars represent two times the propagated standard error of the mean ( $\pm 2 \sigma/\sqrt{n}$ ) of the experimental value. The mean bias over all SZA is shown in red.